Microfluidics processing of piezoelectric and magnetic responsive electroactive microspheres

Luís Amaro Martins[1], **Joaquín Ródenas-Rochina**[1], **Daniel Salazar**[2], **Vanessa F. Cardoso**[3,4], **José Luis Gómez Ribelles**[1,5*] **& Senentxu Lanceros-Mendez**[2,6*]

1 *CBIT – Centre for Biomaterials and Tissue Engineering, Universitat Politècnica de València, 46022 Valencia, Spain; *jlgomez@ter.upv.es*

2 *BCMaterials, Basque Center for Materials Applications and Nanostructures, UPV/EHU Science Park, 48940 Leioa, Spain; *senentxu.lanceros@bcmaterials.net (S.L.M.)*

3 *Center/Department of Physics, Universidade do Minho, 4710-057 Braga*

4 *CMEMS-UMinho, Universidade do Minho, Campus de Azurém, 4800-058 Guimarães, Portugal*

5 *Biomedical Research Networking Center on Bioengineering, Biomaterials, and Nanomedicine (CIBER-BBN), Valencia, Spain*

6 *IKERBASQUE, Basque Foundation for Science, 48009 Bilbao, Spain*

Abstract

Poly(vinylidene fluoride) (PVDF) combined with cobalt ferrites particles (CFO) is one of the most common and effective polymeric magnetoelectric composites. Processing PVDF into its electroactive phase is a mandatory condition for featuring electroactive behavior and specific (post)processing may be needed to achieve this state. However, by processing at a temperature below 60 ºC, electroactive phase crystallization is favored. Besides, different experimental techniques are used to process various forms of PVDF-CFO nanocomposites structures being aware that high CFO dispersion must be achieved. Microfluidics offers the possibility of processing PVDF-CFO microspheres with high reproducibility, size tunability, and time and resources efficiency. Moreover, magnetoelectric microspheres are produced in a one-step approach. Thus, the present work describes the production of high content electroactive phase PVDF and PVDF-CFO microspheres using microfluidic technology. A flow-focusing polydimethylsiloxane (PDMS) device is fabricated based on a 3D printed polylactic acid (PLA) master. The device enables the production of spherical microspheres with mean diameters ranging from 80 and 330 μm depending on the continuous/discontinuous feeding ratio. The microspheres feature internal and external cavernous structures and good CFO distribution with an encapsulation efficacy of 80%. Moreover, the microspheres prove to be in the electroactive γ-phase with a mean content of 75%. Thus, the prepared microspheres show suitable characteristics as active materials for tissue regeneration strategies.

Microfluidics, Microspheres, PVDF, Cobalt Ferrites, Magnetoelectric

Introduction

Polymers are strongly contributing to the development of smart and multifunctional materials. These can execute functions, respond to the environment and exhibit sensory capabilities. Future developments capitalize on technologies able to produce materials exhibiting muscle, brain, and nervous tissue capabilities. Their application is wide, ranging from nanotechnology, biomimetics, neural networking, materials science, and molecular electronics [1].

Piezoelectric polymers are extensively studied due to the ability to produce electric potentials upon mechanical solicitation, and vice-versa [2], [3]. Among them, poly(vinylidene fluoride) (PVDF) gets particular attention due to its high piezoelectric constant, meaning maximal electromechanical transduction [4]. Its intrinsic properties make it useful either as a sensor or as an actuator with no need for bulk and complex external wiring and power sources [3], [5]. PVDF is a semi-crystalline polymer being its crystalline domains responsible for its piezoelectric behavior [5]. When in the electroactive β or γ-phases its molecular arrangement promotes net permanent dipolar moments of the polymer chains thus exhibiting its piezoelectric properties [2].

On the other hand, when subjected to a magnetic field, magnetostrictive particles reorient their magnetic domains changing their shape. Thus, mechanical stimuli are produced upon magnetic solicitation [6], [7]. When embedded in a piezoelectric matrix, these particles enable the production of magnetoelectric composites by coupling their properties and allowing them to act as magnetoelectric transducers [6], [7]. Within the various magnetostrictive particles, cobalt ferrites (CFO) exhibit one of the high magnetostriction, chemical stability and simple processability [7]. The pair PVDF and CFO is then the ultimate choice for the production of polymer magnetoelectric composites [8], [9].

Electrical and mechanical stimulation are common practices in the biological and biomedical fields due to their influence on biological processes [3], [10]. For this reason, both PVDF and PVDF-CFO nanocomposites are largely explored as smart substrates for tissue engineering applications when electrical, mechanical or even electromechanical stimulation can be easily provided in an airtight compartment [2], [3], [11].

The ability of magnetoelectric compounds such as PVDF-CFO nanocomposites to transduce signals, namely magnetic to electric, can be used to produce scaffolds for tissue engineering able to generate surface electric potential variations upon magnetic solicitation, providing with dynamic electrical stimulation the engineered tissues [12] [13]. These functional 3D culture supports emulate the native environment and ECM properties of tissues which are highly dependent on electrical stimulus such as the nervous system, cardiac muscle or bone.

Furthermore, this can be achieved remotely, through magnetic fields, in a very simple manner [12] [13]. The action of an applied magnetic field induces movement and deformation of CFO particles which, in turn, deforms the PVDF polymer matrix and originates an electric field in any point of a 3D culture by surface electric charge density variation at the surface of the microspheres, due to the piezoelectric properties of the material [12] [14]. It is worth noticing that the piezoelectric properties of PVDF are originated by the polar arrangement of its

crystal structure in β or γ crystalline forms. It is thus relevant that the crystallization of PVDF in the microspheres takes place preferentially in any of these phases [15].

Both PVDF and PVDF-CFO have been widely explored as tissue engineering substrates in the form of membranes [16] [17] [18][19] [20], fibers [21] [22] [23] [24] [25] [26] and, in less extent, microspheres [27] [28] [29]or 3D substrates [30] [31], [32] from which only a couple references can be found. In this sense, smart and functional microparticles with piezoelectric and magnetic properties are useful since cells and microparticles can be encapsulated, for instance, in a hydrogel so that cells can be stimulated by mechanical stress and electric fields produced locally.

Both PVDF and PVDF-CFO nanocomposites have been processed by electrospray to form spheres with diameters in the order of a few microns [7], [33] but present some limitations [7], [34]. First of all, the control over microsphere size is difficult and broad size distribution is obtained. On the other hand, the microspheres are collected on a metallic surface on which they tend to agglomerate. The difficulty of collecting and dispersing the microspheres upon production sometimes hinders their applicability. PVDF and their composites have seldom been produced by other common techniques used for the production of polymeric microspheres with only two references found, one for nanoprecipitation and one for emulsion [35] [36].

Microfluidics are miniature fluidic systems composed of reduced channel sizes that originate laminar flows, making them very well suited for the obtention of uniform polymer microspheres [37], [38]. These systems possess several advantages when compared to other common methods for polymer microsphere production [37], [38]. They are automated, fast, have high throughput and allow narrow size microsphere distribution [39], [40]. Thus, microfluidic systems have been fabricated and applied to produce various types of polymer microspheres from polylactic acid, sodium alginate and polycaprolactone, among others, however, unsuccessful when applied to PVDF [41] [42] [43].

In this work, PVDF and PVDF-CFO microspheres are produced employing optimized microfluidic systems built in a simple and reproducible manner using low-cost materials and easily accessible microfluidic processing techniques.

Materials and methods

Materials

PVDF (Solef 6010) and N,N-Dimethylformamide (DMF), pure grade, were supplied by *Solvay* and *Fluka*, respectively. CFO nanoparticles (≈30-55 nm), Triton X-100 and PDMS (Sylgard 184) were purchased from *Nanoamor*, *Sigma-Aldrich* and *Dow Corning*, respectively. Soy lecithin was acquired from *Guinama*. All chemicals were used as received from the suppliers.

Microfluidics system fabrication

Production of PDMS microfluidic systems was performed by replica molding technique. First, microfluidic masters were drawn using free digital modeling software (FreeCAD®), **Erro! A origem da referência não foi encontrada.**a, b.

The design was then processed in a slicing software (*Cura*®) and 3D printed (*Prusa i3 mk3*) with PLA (*FFFWorld PLATech*) over a glass bed. PDMS and activator were thoroughly mixed together in a standard 10:1 ratio. Once degassed in a vacuum chamber, it was poured over the master's and cured in an oven at 40°C for 24 h. The structured PDMS slabs were then removed and cut to size, and the inlets and outlets were punched with an appropriate tool. The PDMS slabs were irreversibly sealed to a glass slide by oxygen plasma (*Piccolo, Plasma Electronics*) following standard procedure [44].

PTFE tubes (1,6 and 0,5mm external and internal diameters respectively) were then inserted into the microfluidic system inlets and outlet and connected to plastic syringes. An Advanced Programmable Syringe Pump from *Harvard Apparatus* and a syringe pump NE-1010 from New Era Pump Systems were used to properly pump fluids into the PDMS microfluidic systems.

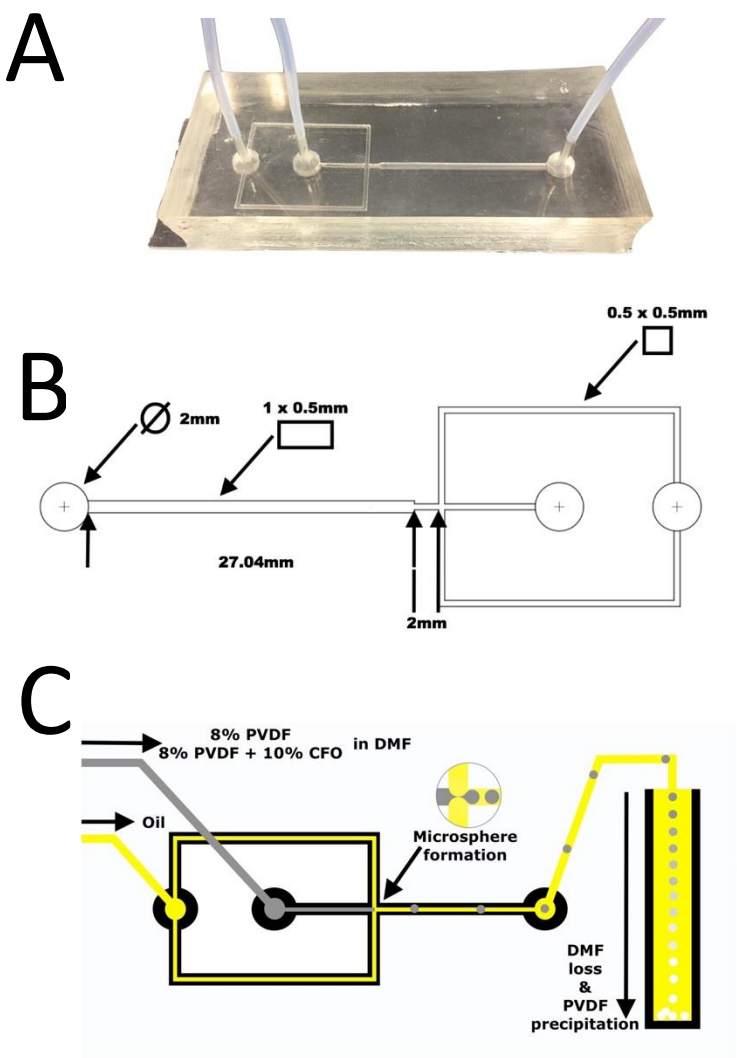

Figure 1 – a) Microfluidic flow-focusing device, b) device's channel dimension c) PVDF and PVDF-CFO microsphere production scheme

Microparticle processing

Sunflower seed oil with 1%(W/V) soy lecithin was used as the continuous medium, as well as the gelifying bath.

For the discontinuous medium, two solutions were prepared to obtain either PVDF or PVDF-CFO microspheres. The concentrations of the polymer and filler were previously optimized to guarantee optimum processing conditions. Thus, for pure PVDF microspheres, an 8%(W/V) PVDF solution in DMF was prepared under magnetic stirring at 80°C for 1 h to achieve fast dissolution [20]. On the other hand, due to the magnetic nature of the CFO particles, the PVDF-CFO solution was prepared differently. CFO was first ultrasonicated in DMF for ½ hour after which the surfactant Triton X-100 at a concentration of 0,02 g/ml was added and left under sonication for an additional 3 and 1/2 h [45]. The bath temperature was turned to 80°C and PVDF was added to the solution. A mechanical PTFE stirrer was then inserted inside, and the solution was left for 1 h extra under both mechanical stirring and ultrasonication ensuring complete polymer dissolution and magnetic particle dispersion. The final product was an 8% PVDF solution with 10%(w/w) CFO relative to the PVDF-CFO blend in DMF. Both solutions were cooled down to room temperature before use.

Syringes were filled with the corresponding continuous and discontinuous mediums, inserted into syringe pumps and primed, these were connected to the corresponding PTFE tubes and pumping was initiated. Continuous and discontinuous mediums were set between 0.05-0.25 ml/min and 0.004-0.020 ml/min, respectively, to change the pressures of the fluid promoting the systematic breakaway of smaller or bigger drops, thus defining the final microspheres dimensions, droplet formation was unstable for values outside the range.

After production inside the microfluidic device, the microdroplets were dropped in a vertical glass column filled with the above-mentioned oil solution as exemplified in **Erro! A origem da referência não foi encontrada.**c. The microspheres were recovered from the bottom of the column after 24 h ensuring complete solvent removal. Once recovered the microspheres were thoroughly washed with acetone first to remove any oil remnants, and then water to remove any acetone residues. After being left to dry overnight they were ready to use.

Sample characterization

Surface images were acquired in a *Zeiss Ultra 55* Field Emission Scanning Electron Microscope (FE-SEM) at 1kV power without coating.

Internal images were taken with a *Zeiss* Focused Ion Beam (FIB) *Auriga Compact*. Cuts were performed with an argon ion beam at 2μA and the pictures were taken at 5kV. To observe the interior of the microspheres, the samples were previously carbon coated in a *Leica EM MED 020* sputter to enhance contrast.

Microsphere diameters were digitally measured with *ImageJ* analysis software. Pictures for the dimension assay were taken with a tabletop stereo microscope *Leica MZ APO*. 50 microspheres were measured, and the results are provided as mean diameter and standard deviation.

Fourier-transform infrared spectroscopy (FTIR) spectra were acquired in a *Bruker Alpha II* FTIR Spectrometer in the Attenuated Total Reflectance (ATR) mode. Spectra were collected from 128 scans at 4 cm^{-1} resolution, between 400 and 4000 cm^{-1}. Differential scanning calorimetry (DSC) thermograms were recorded on a *Perkin Elmer 8000* DSC. Samples were sealed in aluminum pans. A baseline, obtained by measuring an empty aluminum pan, was subtracted from the original samples thermograms. The analysis was performed under nitrogen (N_2) purge at 20 mL/min from 30 to 200 °C at a 20 °C/min heating rate. Thermogravimetric analysis (TGA) was performed on a *Mettler Toledo* TGA analyzer. Alumina pans were used to hold the samples. The analysis was performed under an N_2 atmosphere at 50mL/min from 30 to 800°C at a 10°C/min heating rate in order to optimize the scan resolution. Magnetic properties were assayed at room temperature in a *MicroSense EZ7-VSM* vibrating sample magnetometer (VSM) from -18 to 18 kOe.

Microspheres disinfection and preconditioning

Previous to cell culturing, the microspheres were disinfected with 70% ethanol to eliminate possible microorganisms. The protocol applied was as follows, PVDF microspheres were incubated with 100% ethanol for 10 minutes, followed by a double incubation in 70% ethanol for 10 minutes and finally incubated overnight with 70% ethanol. To remove the ethanol, microspheres were washed for 10 minutes in decreasing ethanol/water dilutions, 50/50, 30/70, 10/90 and finally 0/100. To improve cell adhesion materials were incubated with Dubelcco's Modified Eagle Medium (DMEM) high glucose (Fisher) supplemented with 1% (V/V) of penicillin/streptomycin (Fisher) and 10% (V/V) fetal bovine serum (Gibco). This final step was carried out overnight in an incubator at 37ºC. All the steps above were performed with a *Grant-Bio PTR-35* microcentrifuge tube vertical rotator.

Cell expansion and cytotoxicity assay

Microspheres metabolic and cytotoxic effects were evaluated through direct contact with rabbit chondrocytes (RC) by the (3-(4,5-dimethylthiazol-2-yl)-5-(3-carboxymethoxyphenyl)-2-(4-sulfophenyl)-2H-tetrazolium) (MTS) colorimetric assay, assessing the materials biocompatibility and CFO retention. RC's were used since they are a precursor line to cartilaginous tissue and one of the targets for electrically stimulated tissue culture [3] [46]. RCs were expanded until passage 5 with DMEM high glucose culture medium (Fisher) enriched with 1% (V/V) of penicillin/streptomycin (Fisher), 1% (V/V) sodium pyruvate (Fisher), 10% (V/V) of fetal bovine serum (Gibco) and 50 µg/ml ascorbic acid (Sigma- Aldrich), cells were collected and concentrated to $0.4x10^6$ cells/ml and combined with 0.02% (v/v) PVDF (66µm) or PVDF-CFO (52µm) microspheres. Cells with PVDF, PVDF-CFO or only cells (control) were seeded by transferring 500 µl of the cell suspension to 500 µl microtubes and centrifuged at 1000 rpm for 5 minutes to allow micromasses formation with a final diameter of around 1 mm. Cell micromasses were cultured at 37ºC and 5% CO_2. At 24 and 72 hours, 3 samples of each group were removed, washed with Dubelcco's Phosphate Buffers Saline (DPBS) and placed in a 24 well plate. Each sample and control was covered with 400 µl of MTS reagent

diluted in DMEM high glucose (1:10) without phenol red and incubated at 37ºC and 5% CO_2 for 2 hours and 30 minutes. As inner control 3 empty culture wells were filled with 400 µl of MTS reagent. Finally, colorimetric measurements of the formazan dye were performed on a *Victor3* spectrometer at 490 nm. Results were expressed as relative MTS activity as compared to control conditions. All essays were performed in triplicates to ensure their statistical relevance.

Results and discussion

Flow-focusing microfluidic systems use an immiscible fluid to systematically break the polymer solution into small droplets. These naturally take a spherical shape due to its isotropic nature, fluids tending to reach equilibrium minimizing the system's free energy and achieving thermodynamic stability [47], [48]. The channels dimensions in the micrometer range guarantee a continuous laminar flow thus producing monodisperse droplets.

Polymer precipitation is achieved through phase inversion, since DMF and sunflower oil mix slowly, while still allowing droplet formation at the channels crossing point. Droplets are then dropped on an oil-filled vertical column, the spherical shape is maintained while the polymer slowly precipitates and crystallizes due to the gradual solvent diffusion to the oil medium, as exemplified in **Erro! A origem da referência não foi encontrada.**c, reaching the bottom as solid polymer microspheres.

Morphological analysis

Representative FESEM and FIB images of PVDF and PVDF-CFO microspheres processed by microfluidic technology are presented in Figure 2.

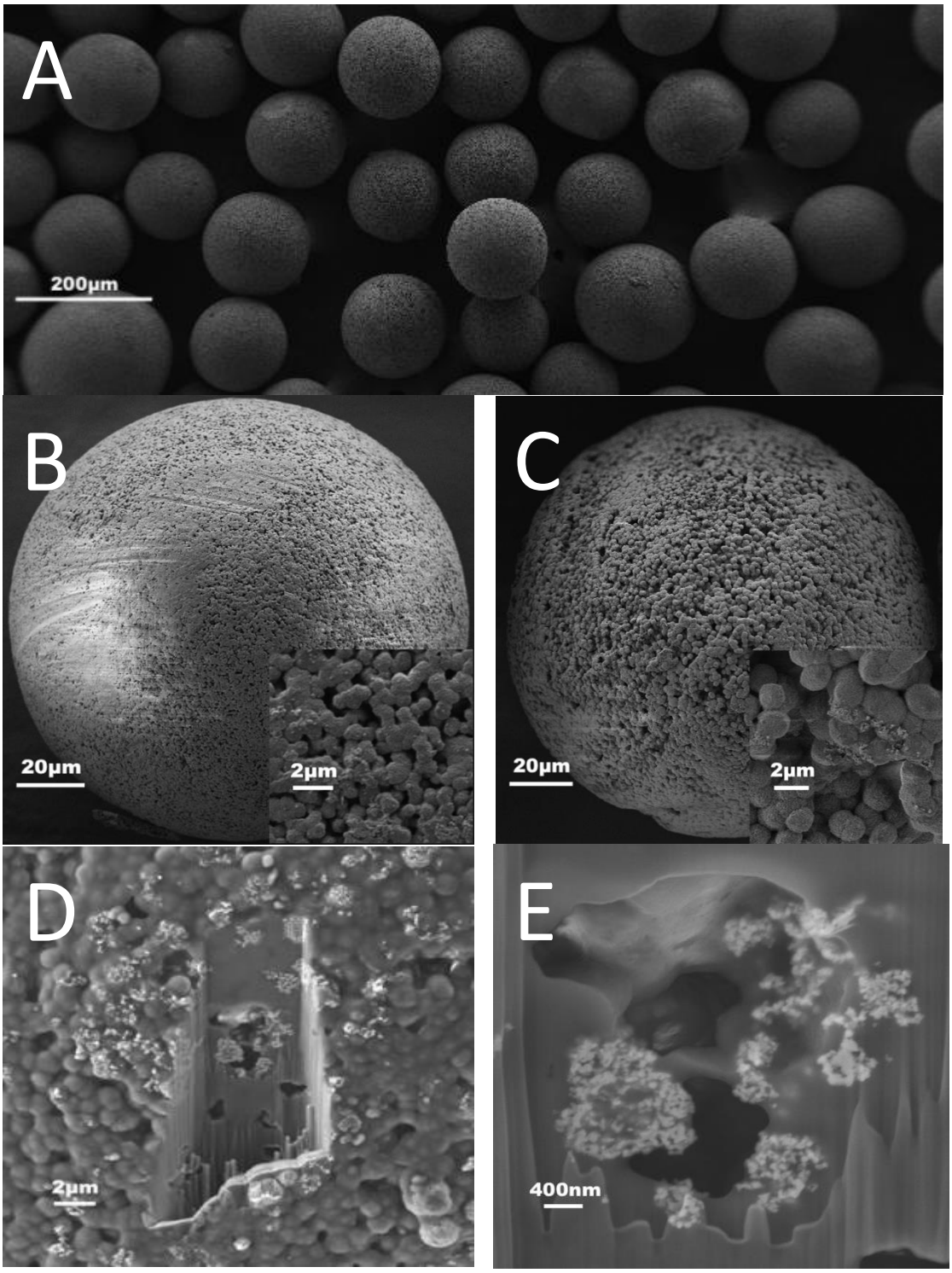

Figure 2 – FESEM images of a) various PVDF microspheres, b, c) PVDF and PVDF-CFO microspheres, respectively, with insets of surface details, and d, e) a FIB cross-sectioned PVDF-CFO microsphere.

Both samples, PVDF and PVDF-CFO, exhibit a spherical shape without visible defects. The surfaces, detailed in the insets, feature a textured and porous morphology in both samples, resembling an aggregate of micron size microspheres. These structures are associated to PVDF spherulites formed from solution, as occurred in PVDF membranes obtained by non-solvent induced phase separation

using low temperature coagulation bath [49] [50]. On PVDF-CFO samples, CFO are presented on the surface of the microspheres, as can be seen on the inset of Figure 2c. Distribution is even with small CFO nanoparticle clusters uniformly distributed throughout the surface.

The FIB cross-sectioned FESEM images of the PVDF-CFO microspheres, Figure 2d, shows that CFO nanoparticles distribution is organized in small clusters spread throughout the sample. Thus, both surface and cross-section images indicate good particle dispersion. Moreover, pores can be observed on the inside and surface of the microspheres indicating a cavernous internal structure extending all way through the microsphere. Confocal microscope imagens of PVDF-CFO microspheres add a more detailed look on surface morphology and crystallite structures and are available as supporting material.

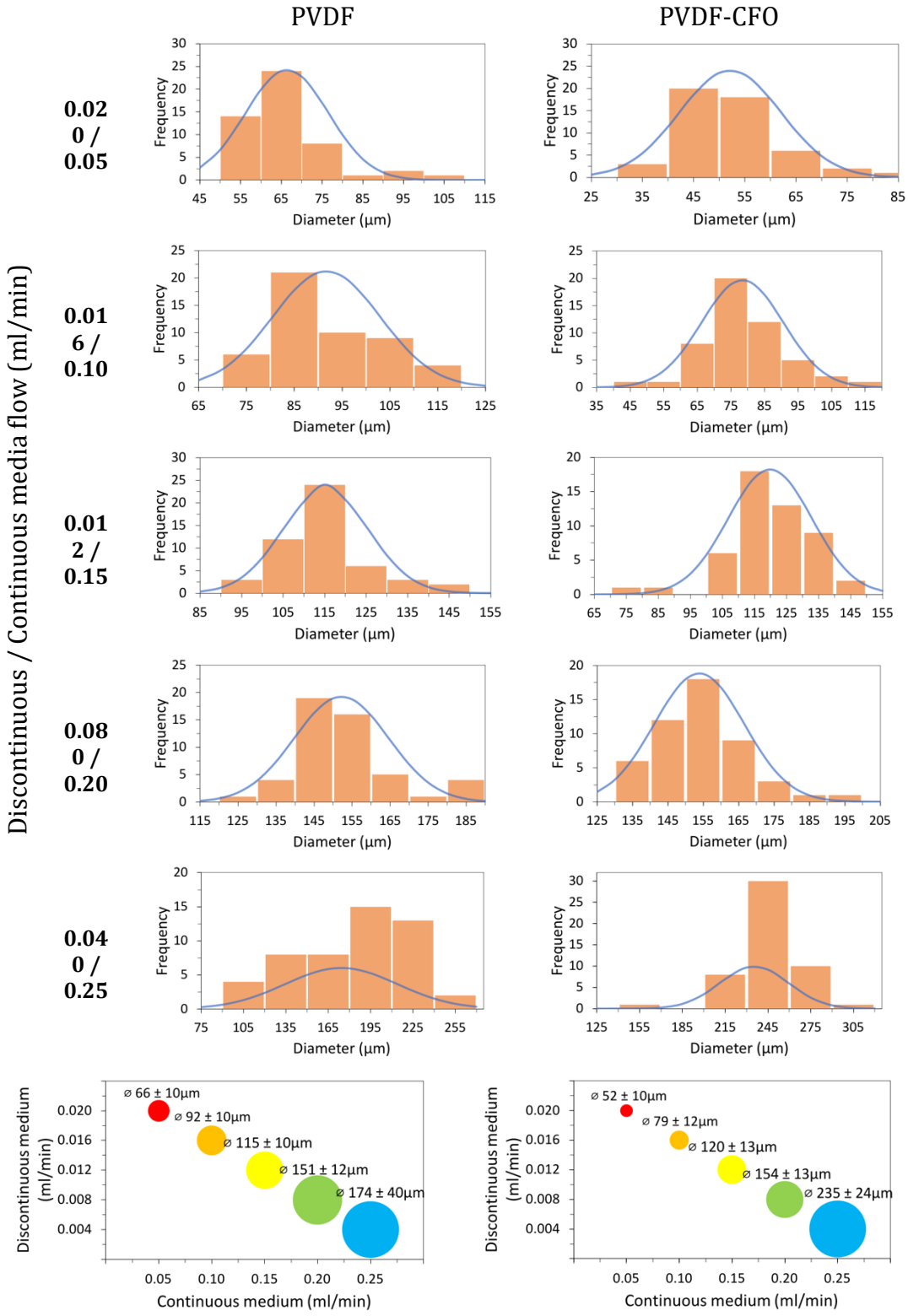

Figure 3 – Histograms of PVDF and PVDF-CFO microsphere diameter for the diverse processing parameters (n=50) (top), Microsphere diameter dependence on processing parameters (bottom)

The microfluidic system is able to produce microspheres in a wide range of sizes from 66 to 174µm for PVDF and 52 to 235µm for PVDF-CFO by tuning the flow

ratio of continuous to discontinuous medium between 62.5 and 2.5, respectively. Higher ratios between continuous and discontinuous media produce microspheres with smaller dimensions. Below and above said ratios the systems behavior became instable, being unable to produce droplets or losing the spherical shape by colliding with the systems walls. Size distribution, average size and standard deviation of the microspheres produced are exhibited in **Erro! A origem da referência não foi encontrada.**. Differences in microsphere diameter between PVDF and PVDF-CFO samples have been observed for the same processing conditions, probably due to the magnetic attraction among CFO particles altering solution properties and behavior. Previous to collection microspheres were sieved in order to remove the largest aggregates.

The produced microspheres did not achieve the level of monodispersity commonly associated with microfluidics, although dispersity, is far superior to the size distribution of electrosprayed microspheres [7]. Since the system operates under a laminar flow regime, microdroplet separation occurs in a systematic and repeatable manner, generating monodisperse droplets, but coalescence happens due to the flowing nature of the continuous medium and the static nature of the precipitation column making droplets experiencing a flow reduction and coalescence while going from one to the other. Coalesced droplets dropped faster and consequently coalesced with other non-precipitated droplets on their way, leading to a snow-man effect. This fact could be avoided manually by distributing the droplets through the column surface, although leading to a labor-intensive process, which could be automated leading to increased monodispersity.

Physical and chemical characteristics

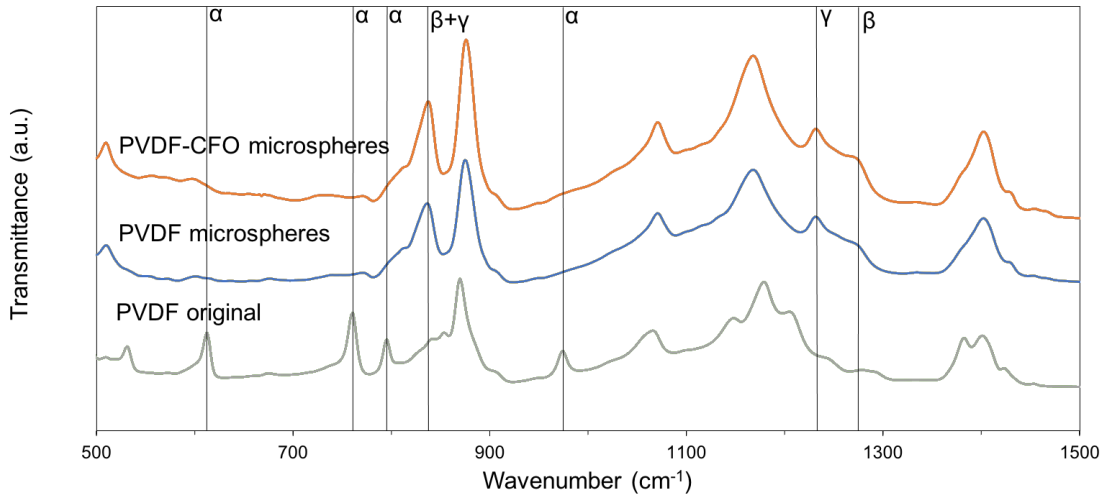

Figure 4 - FTIR spectra for the PVDF and PVDF-CFO microspheres. Original PVDF pellets spectrum is also shown for comparison

The Infrared spectra (IR) of the PVDF and PVDF-CFO microspheres can be observed in **Erro! A origem da referência não foi encontrada.**. The spectrum of the original PVDF pellets, is also included. The polymers chemical structure is

composed of repeating -CH_2-CF_2- units. α, β and γ-phases identification is possible by their characteristic vibrational modes described in Table 1 [33], [51], [52].

Table 1 - PVDF and corresponding crystal phase IR specific peaks.

Crystalline structure	Characteristic peaks (cm^{-1})	Vibrational mode
α-phase	614	CF_2 Stretching
	763	CF_2 Stretching
	795	CH_2 Stretching
	975	CH Stretching
β-phase	1276	CF Stretching
	840	CH_2 Stretching
γ-phase	1234	CF_2 Stretching

The characteristic peaks of the α-phase are clearly shown in the original PVDF, which shows intense peaks at 614 and 763cm^{-1}, **Erro! A origem da referência não foi encontrada.**4 [51]. Nevertheless in PVDF microspheres, with or without CFO, the predominant phase is the γ-phase, as observed by the presence of the intense 1234cm^{-1} peak [51], [52].

The fractions of α, and electroactive phase (EA), β and γ, can be determined using **Erro! A origem da referência não foi encontrada.**,

$$F(\mathrm{EA}) = \frac{A_{\mathrm{EA}}}{\left(\frac{K_{\mathrm{EA}}}{K_{\alpha}}\right) A_{\alpha} + A_{\mathrm{EA}}} \qquad \textit{Equation 1}$$

where F(EA) is the percentage of EA-phase, A_α and A_{EA} are the baseline corrected absorbance at 766 and 840cm^{-1}, respectively and K_α and K_{EA} the absorbance coefficients of the respective peaks at 6.1×10^4 and 7.7×10^4cm/mol [7], [53].

A deconvolution of the FTIR spectra in the regions between 1140 and 1300cm^{-1} for the PVDF and PVDF-CFO microspheres was performed in order to isolate specific β and γ-phase peaks, as shown in Figure 55.

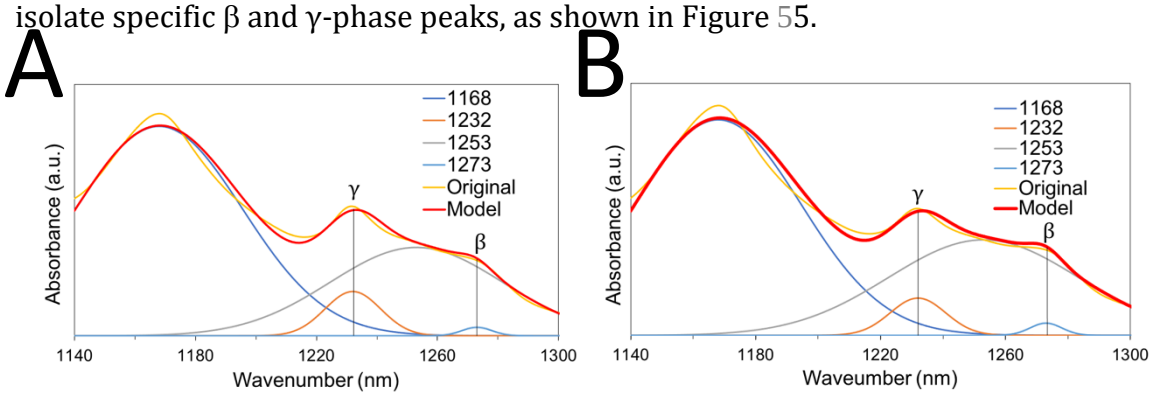

Figure 5 - FTIR spectra deconvolution for a) PVDF and b) PVDF-CFO microspheres between 1140-1300cm^{-1}.

The percentages of individual contributions of β and γ structures to the EA-phase can be calculated by **Erro! A origem da referência não foi encontrada.**,

$$F(\gamma) = F(EA) \times \left(\frac{A_\gamma}{A_\gamma + A_\beta}\right) \times 100 \qquad \textit{Equation 2}$$

where F(γ) is the γ-phase percentage, F(EA) the electroactive phase percentage and A_γ and A_β the 1234 and 1275 cm^{-1} peaks relative absorption intensities [51].

PVDF and PVDF-CFO microspheres are mainly crystallized in the γ-phase. This phase represents a polar arrangement of the polymer structure where the highly electronegative F forms a C-F bond with significant dipole moment originating its piezoelectric effect. This phase is characterized by an orthorhombic unit cell with a TTTGTTTG' sequence of trans and gauche conformation [54] [55].

Solvent type, hydrostatic pressure and presence of surfactants are known to modulate crystallization kinetics and induce γ-phase crystallization in PVDF films [56], [57]. On PVDF films processed by the NIPS method (similar to the developed microfluidics precipitation method) γ, β and α phases can be produced independently of the diffusion rate. Solvent-antisolvent dipole-moment interactions are deemed to be the major fact affecting PVDF crystallization. Increasing dipole-moment sequentially produced α, γ and β structures while it was common for samples to exhibit a combinations of them [58].

In order to yield such high values of γ-phase, PVDF processing techniques commonly rely on high temperatures, additives or post-processing. Further, these processes are only applied to films and would be particularly difficult to apply to other morphologies, specially microspheres due to the lack of flat surfaces [52], [59].

In the analysis of the FTIR spectrum shown in Figure 5 - FTIR spectra deconvolution for a) PVDF and b) PVDF-CFO microspheres between 1140-1300cm^{-1}.Figure 5, comparison between the ratio of γ to β peaks intensity in the different samples, given by F(γ) in Equation 2, could be more significant than the comparison of the absolute values of the peaks area of each one. It can be observed that the presence of CFO nanoparticles increases slightly F(γ) from 73% to 75%. This slight difference in γ-phase content between samples is possibly explained by the interaction between the negative zeta potential of the CFO particles and the positively charged CH_2 groups increasing γ-phase nucleation [9], [60], [61]. The mechanism seems valid for crystallization in a polar arrangement, β or γ in the presence of positively charged particles contributing to the polymer's polar arrangement.

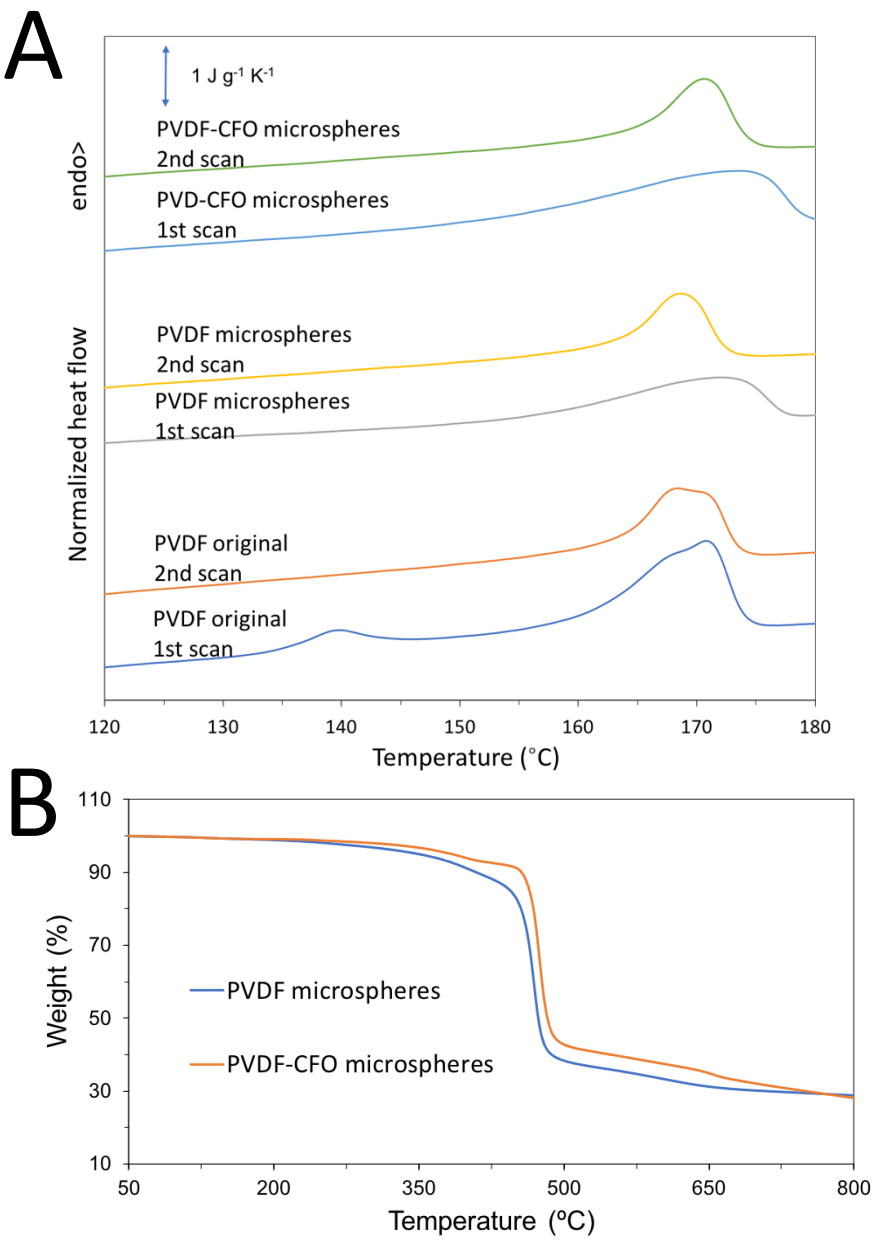

Figure 6 - a) DSC spectra for the PVDF and PVDF-CFO microspheres, b) TGA spectra for the PVDF and PVDF-CFO microspheres

Thermal properties of the PVDF and PVDF-CFO samples were studied by DSC calorimetric curves and analyzed in terms of their thermal parameters: melting temperature (T_m), melting enthalpy (ΔH_s) and the crystalline fraction (Xc). The melting process is characteristically observed in DSC calorimetry as an endothermic peak. Tm was established as the peaks maximum, as in **Erro! A origem da referência não foi encontrada.**, in addition, Xc was calculated according to **Erro! A origem da referência não foi encontrada.**,

$$Xc(\%) = \frac{\Delta H_s}{x\Delta H_\alpha + y\Delta H_\beta + z\Delta H_\gamma} x100 \qquad \textit{Equation 3}$$

where Xc stands for the sample crystalline fraction, ΔH_s for the PVDF melting enthalpy, corresponding to the melting peak's area, x, y and z stand for the percentage of α, β and γ-phases, respectively and were calculated by Equation 2, 3, and ΔH_α, ΔH_β and ΔH_γ are the melting enthalpies for a 100 % crystalline sample in the respective phases. ΔH_α , ΔH_β , and ΔH_γ ,were considered as 93.07, 103.40 and 104.60 J/g, respectively [61], [62]. Thermal parameters are summarized in Table 2.

Table 2 - Thermal parameters and content of crystal phases of PVDF and PVDF-CFO.microspheres

	PVDF	**PVDF-CFO**
T_m (°C)	171	172
ΔH_s (J/g)	44	64
F_α (%)	12	10
F_β (%)	15	15
F_γ (%)	73	75
Xc (%)	44	63

All thermograms are characterized by a single endothermic peak, T_m. Fusion temperature is low for γ crystalline structures that usually melt at higher temperatures, probably due to crystallization at room temperature since usually much higher temperatures are used to achieve γ-phase crystallization [52].

First and second heat scans behave similarly whether PVDF or PVDF-CFO are regarded. Three main differences can be observed when comparing the melting peaks from structures crystallized from solution and from the melt. Solution crystallized peaks are wider, lower in energy and have higher T_m. These reflect the differences in the crystalline structure under different crystallization conditions.

Wider peaks indicate a distribution of crystallites with different sizes in the solution crystallized samples. On the other hand, T_m is dependent on crystallites lamellae thickness, confirming different crystal sizes forming from the melt or solution, as previously mentioned. The higher fusion enthalpy of the first heat fusion peak correlates to the presence of more ordered structures thus less amorphous portions and higher crystallinity [63].

It is frequent that double peaks appear in the DSC heating scans of PVDF [64] and other semicrystalline polymers [65]. They can be ascribed to the presence of different co-existing crystalline phases, but also to the recrystallization of the polymer chains during the heating scan itself. Crystallization at low temperatures produces small lamellae that in turn melts at low temperatures. During the heating scan, melting starts at temperatures still in the range of temperatures that allow crystallization. When this happens, an exothermal crystallization peak overlaps on the melting endotherm and the results seems a double melting peak [66].

One can only speculate about the spectrum of the original ground polymer since the thermal history of its crystallization process is not known. Nevertheless, it is quite interesting to observe the melting endotherm of the microspheres in the first heating scan. In spite that the microspheres are formed in the microfluidics process at room temperature, so with a very low crystallization temperature, the melting endotherm appears as a quite broad peak with a maximum at a temperature higher than in the original PVDF and also higher than in the second scan in which PVDF chains crystallizes preferentially in α-phase. The previous discussion would made one to expect that melting start in the heating scan at lower temperatures than in the second one. The observed behavior is an additional proof that in the microspheres PVDF is crystallized in γ-phase which has a melting temperature higher than α-phase [52] [67].

T_m is around the same value for both samples and in accordance with other articles [7]. This way it is possible to conclude that neither processing in a microfluidics system nor the addition of 10 % CFO pose any significant changes in the polymer's T_m [7], [62].

Differences in Xc can be correlated with CFO addition due to CFO presence acting as nucleation centers for crystallite formation in PVDF [7], [60], [68].

In **Erro! A origem da referência não foi encontrada.**b the typical PVDF two-step degradation curve can be observed for both samples as stated elsewhere [7], [69]. PVDF sample exhibited a lower onset temperature, 463 °C, relative to PVDF-CFO, 475 °C, revealing increased thermal stability with CFO addition, as previously mentioned [7], [70]. The degradation step between ≈370°C and ≈470°C in PVDF-CFO is attributed to the degradation of Triton X-100 remaining in the microspheres, thus being absent in the PVDF sample [71]. The remaining mass can be explained by the non-volatile residues left after polymer pyrolysis.

The hysteresis loop obtained at room temperature for the PVDF-CFO microspheres and illustrated in **Erro! A origem da referência não foi encontrada.** revealed a magnetization of 4,3 emu/g, coercivity (Hc) of 2.8 kOe, and ferromagnetic behavior, as expected. Figure 7 on the inset. The hysteresis loop for pure CFO particles is also presented, revealing a magnetization of 54,5 emu/g, and coercivity (Hc) of 2.6 kOe. Similar values of Hc indicate that the CFO nanoparticles were not modified or degraded during the processing of the PVDF-CFO microspheres Mass percentage of magnetic particles in the sample was calculated according to Equation 4, where M_c, is the normalized saturation magnetization of the pure CFO particles, M_s, the sample's normalized saturation magnetization and MP(%), the mass percentage of magnetic particles in the sample.

$$MP(\%) = \frac{Ms}{Mc} \times 100 \qquad \textit{Equation 4}$$

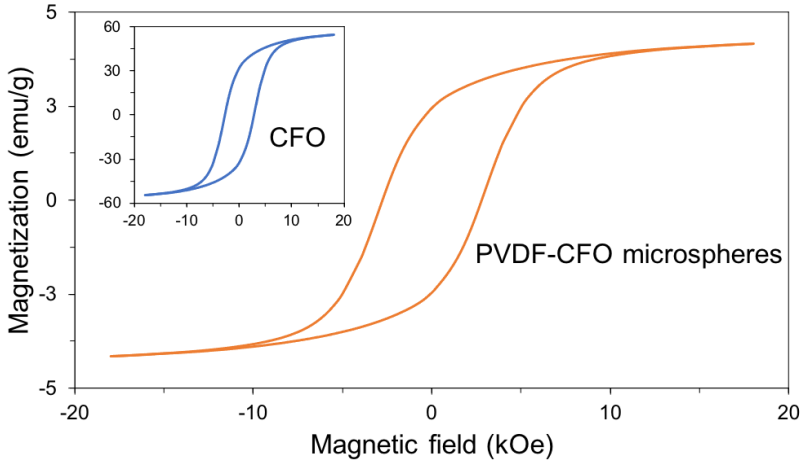

Figure 7 - Hysteresis loop for PVDF-CFO microspheres and inset for pure CFO.

Having into account the saturation magnetization values of pure CFO and PVDF-CFO samples, the mass percentage of magnetic particles in the sample was calculated to be 8 %. Encapsulation efficacy (Ee) expresses a measurement, in %, of CFO particle incorporation into polymers matrix during microsphere processing. It can be calculated from Equation 5, where MP stands for the mass percentage of magnetic particles in the sample and MPt stands for the mass percentage of magnetic particles incorporated into the polymer solution before processing. The Ee of PVDF-CFO processing is 80%, which is correlated to a 20% particle loss during processing, as magnetic particles tend to form dense aggregates that precipitate at the syringe bottom. Previous works of PVDF-CFO composite microspheres processed through electrospray exhibit particles loss in the order of 50 % showing the superior particle retention of the developed processing method [7].

$$Ee(\%) = \frac{MP}{MPt} \times 100 \qquad \textit{Equation 5}$$

Metabolic activity assay

MTS results of 3D cultured rabbit chondrocytes (RC) micromasses are summarized in **Erro! A origem da referência não foi encontrada.**. RC micromasses surpassed the control's metabolic activity when cultured with PVDF and PVDF-CFO microspheres for both 24 and 72 h essays. MTS values for 24 h essay registered values of 1.2 and 1.6-fold the control for PVDF and PVDF-CFO, respectively. The 72 h essays registered closer values of approximately 1.3-fold for both PVDF and PVDF-CFO. The later essay also registered lower standard deviation values than the former.

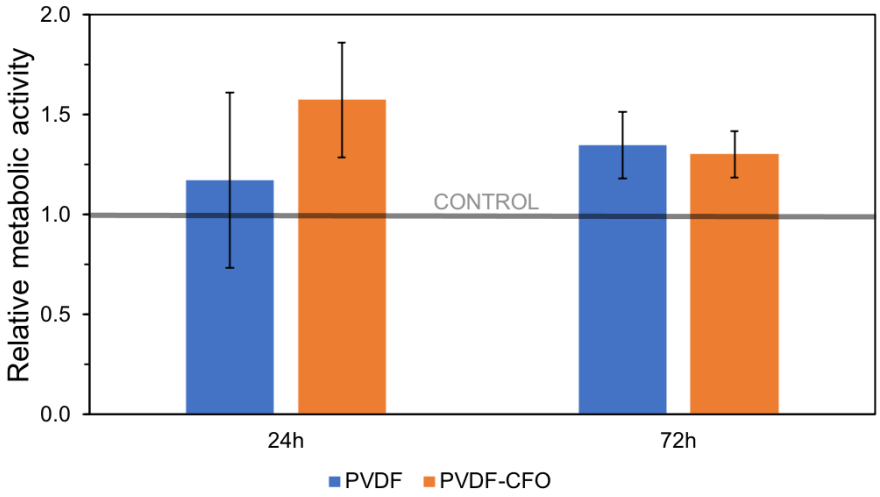

Figure 8 - MTS Relative metabolic activity for PVDF and PVDF-CFO microspheres at 24 and 72 h culture times.

Metabolic activity of RC was improved by a minimum of 1.2-fold in the presence of PVDF or PVDF-CFO microspheres thus demonstrating its enhancement relative to the control, hence microsphere absence, thus proving the materials cytocompatibility on direct contact. Although CFO's cytotoxic effects are described in the literature, in our case no negative effects were observed even though CFO clusters were observed on the PVDF-CFO microsphere's outer and inner surfaces, Figure 2, thus proving the strong encapsulation/retention provided by the polymer's matrix during culture conditions [72], [73].

Conclusions

The proposed method based on microfluidic technology enables the production of narrow size dispersion PVDF and PVDF-CFO nanocomposite microspheres with a size range between 52 and 235 μm. The obtained microspheres exhibited a homogeneous and round shape and textured surface with good CFO particle dispersion and retention efficacy of 80 %. Moreover, the samples exhibit high electroactive γ-phase content of 75 %, and crystallinity between 44 and 64 %, thus not requiring post-processing thermal treatments. Other thermal and chemical properties are on par with conventional processing methods. 3D culture of RC micromasses promoted and 1.2-1.7-fold increase in metabolic activity in the presence of PVDF and PVDF-CFO microspheres.

This way, the proposed microfluidic approach is innovative, simple and cost- and time effective while producing highly electroactive PVDF and PVDF-CFO microspheres in large quantities in an autonomous manner that is easy to collect and manipulate, surpassing other methods available today, such as electrospray. Moreover, the systems are fabricated using a common 3D printer and replica molding techniques available in most laboratories.

Our method is superior for producing electroactive PVDF and PVDF CFO microspheres allying easy and controllable manufacturing with time, resources, and product reduction benefits with increased bioactivity.

Acknowledgments

This work has been funded by the Spanish State Research Agency (AEI) through the projects PID2019-106099RB-C41 and C43/AEI/10.13039/501100011033. CIBER-BBN is an initiative funded by the VI National R&D&I Plan 2008–2011, Iniciativa Ingenio 2010, Consolider Program. CIBER Actions are financed by the Instituto de Salud Carlos III with assistance from the European Regional Development Fund. V.F.C. also thanks to the Portuguese Foundation for Science and Technology (FCT) for financial support under the Assistant Researcher Contract 2020.02304.CEECIND. The authors also acknowledge funding from the Basque Government Industry and Education Departments under the ELKARTEK and PIBA (PIBA-2018-06) programs, respectively.

The author also thanks to the microscopy service of the Universitat Politècnica de València for all the help, patience and attention.

Data availability

The raw data required to reproduce these findings cannot be shared at this time due to technical or time limitations.

References

[1] M. V Gandhi and B. D. Thompson, *Smart materials and structures*. Springer Science & Business Media, 1992.

[2] K. S. Ramadan, D. Sameoto, and S. Evoy, "A review of piezoelectric polymers as functional materials for electromechanical transducers," *Smart Materials and Structures*, vol. 23, no. 3, p. 33001, 2014.

[3] C. Ribeiro, V. Sencadas, D. M. Correia, and S. Lanceros-Mendez, "Piezoelectric polymers as biomaterials for tissue engineering applications," *Colloids and Surfaces B: Biointerfaces*, vol. 136, pp. 46–55, 2015, doi: 10.1016/j.colsurfb.2015.08.043.

[4] E. Fukada, "Recent developments of polar piezoelectric polymers," *IEEE transactions on dielectrics and electrical insulation*, vol. 13, no. 5, pp. 1110–1119, 2006.

[5] V. Sencadas, R. Gregorio Jr, and S. Lanceros-Méndez, "α to β phase transformation and microestructural changes of PVDF films induced by uniaxial stretch," *Journal of Macromolecular Science®*, vol. 48, no. 3, pp. 514–525, 2009.

[6] G. Srinivasan, "Magnetoelectric Composites," *Annual Review of Materials Research*, vol. 40, no. 1, pp. 153–178, 2010, doi: 10.1146/annurev-matsci-070909-104459.

[7] R. Gonçalves *et al.*, "Development of magnetoelectric CoFe 2 O 4/poly (vinylidene fluoride) microspheres," *RSC Advances*, vol. 5, no. 45, pp. 35852–35857, 2015.

[8] S. Amiri and H. Shokrollahi, "The role of cobalt ferrite magnetic nanoparticles in medical science," *Materials Science and Engineering: C*, vol. 33, no. 1, pp. 1–8, 2013.
[9] R. Gonçalves *et al.*, "Magnetoelectric CoFe 2 O 4/polyvinylidene fluoride electrospun nanofibres," *Nanoscale*, vol. 7, no. 17, pp. 8058–8061, 2015.
[10] A. H. Rajabi, M. Jaffe, and T. L. Arinzeh, "Piezoelectric materials for tissue regeneration: A review," *Acta Biomaterialia*, vol. 24. pp. 12–23, 2015. doi: 10.1016/j.actbio.2015.07.010.
[11] C. Ribeiro, D. M. Correia, S. Ribeiro, V. Sencadas, G. Botelho, and S. Lanceros-Méndez, "Piezoelectric poly (vinylidene fluoride) microstructure and poling state in active tissue engineering," *Engineering in Life Sciences*, vol. 15, no. 4, pp. 351–356, 2015.
[12] C. Ribeiro, V. Correia, P. Martins, F. M. Gama, and S. Lanceros-Mendez, "Proving the suitability of magnetoelectric stimuli for tissue engineering applications," *Colloids and Surfaces B: Biointerfaces*, vol. 140, pp. 430–436, 2016.
[13] N. D. Ferson, A. M. Uhl, and J. S. Andrew, "Piezoelectric and magnetoelectric scaffolds for tissue regeneration and biomedicine: a review," *IEEE Transactions on Ultrasonics, Ferroelectrics, and Frequency Control*, vol. 68, no. 2, pp. 229–241, 2020.
[14] S. Reis, M. Silva, P. Martins, and S. Lanceros-Mendez, "Applications of Polymer-Based Magnetoelectric Materials: Sensors, Actuators, Antennas, and Memories," *Magnetoelectric Polymer-Based Composites: Fundamentals and Applications*, pp. 153–170, 2017.
[15] P. Martins and S. Lanceros-Méndez, "Polymer-based magnetoelectric materials," *Advanced Functional Materials*, vol. 23, no. 27, pp. 3371–3385, 2013.
[16] C. Ribeiro *et al.*, "Fibronectin adsorption and cell response on electroactive poly (vinylidene fluoride) films," *Biomedical Materials*, vol. 7, no. 3, p. 035004, 2012.
[17] P. M. Martins *et al.*, "Effect of poling state and morphology of piezoelectric poly (vinylidene fluoride) membranes for skeletal muscle tissue engineering," *Rsc Advances*, vol. 3, no. 39, pp. 17938–17944, 2013.
[18] C. Ribeiro *et al.*, "Enhanced proliferation of pre-osteoblastic cells by dynamic piezoelectric stimulation," *Rsc Advances*, vol. 2, no. 30, pp. 11504–11509, 2012.
[19] S. Ribeiro *et al.*, "Magnetically activated electroactive microenvironments for skeletal muscle tissue regeneration," *ACS Applied Bio Materials*, vol. 3, no. 7, pp. 4239–4252, 2020.
[20] M. Guillot-Ferriols *et al.*, "Poly (vinylidene) fluoride membranes coated by heparin/collagen layer-by-layer, smart biomimetic approaches for mesenchymal stem cell culture," *Materials Science and Engineering: C*, vol. 117, p. 111281, 2020.
[21] P. M. Martins *et al.*, "Effect of poling state and morphology of piezoelectric poly (vinylidene fluoride) membranes for skeletal muscle tissue engineering," *Rsc Advances*, vol. 3, no. 39, pp. 17938–17944, 2013.
[22] M. M. Maciel *et al.*, "Relation between fiber orientation and mechanical properties of nano-engineered poly (vinylidene fluoride) electrospun

composite fiber mats," *Composites Part B: Engineering*, vol. 139, pp. 146–154, 2018.
[23] M. Kitsara *et al.*, "Permanently hydrophilic, piezoelectric PVDF nanofibrous scaffolds promoting unaided electromechanical stimulation on osteoblasts," *Nanoscale*, vol. 11, no. 18, pp. 8906–8917, 2019.
[24] E. Esmaeili *et al.*, "Magnetoelectric nanocomposite scaffold for high yield differentiation of mesenchymal stem cells to neural-like cells," *J Cell Physiol*, vol. 234, no. 8, pp. 13617–13628, 2019.
[25] S. Wu, M.-S. Chen, P. Maurel, Y. Lee, M. B. Bunge, and T. L. Arinzeh, "Aligned fibrous PVDF-TrFE scaffolds with Schwann cells support neurite extension and myelination in vitro," *J Neural Eng*, vol. 15, no. 5, p. 056010, 2018.
[26] P. Hitscherich, S. Wu, R. Gordan, L. Xie, T. Arinzeh, and E. J. Lee, "The effect of PVDF-TrFE scaffolds on stem cell derived cardiovascular cells," *Biotechnol Bioeng*, vol. 113, no. 7, pp. 1577–1585, 2016.
[27] D. M. Correia *et al.*, "Electrosprayed poly (vinylidene fluoride) microparticles for tissue engineering applications," *Rsc Advances*, vol. 4, no. 62, pp. 33013–33021, 2014.
[28] R. Sobreiro-Almeida *et al.*, "Human mesenchymal stem cells growth and osteogenic differentiation on piezoelectric poly (vinylidene fluoride) microsphere substrates," *Int J Mol Sci*, vol. 18, no. 11, p. 2391, 2017.
[29] B. Hermenegildo *et al.*, "Hydrogel-based magnetoelectric microenvironments for tissue stimulation," *Colloids and Surfaces B: Biointerfaces*, vol. 181, pp. 1041–1047, 2019.
[30] M. M. Fernandes, D. M. Correia, C. Ribeiro, N. Castro, V. Correia, and S. Lanceros-Mendez, "Bioinspired three-dimensional magnetoactive scaffolds for bone tissue engineering," *ACS Appl Mater Interfaces*, vol. 11, no. 48, pp. 45265–45275, 2019.
[31] S. M. Damaraju *et al.*, "Three-dimensional piezoelectric fibrous scaffolds selectively promote mesenchymal stem cell differentiation," *Biomaterials*, vol. 149, pp. 51–62, 2017.
[32] M. Kitsara *et al.*, "Plasma-modification of PVDF Scaffolds improve Cardiomyocytes Viability and Morphology".
[33] D. M. Correia *et al.*, "Electrosprayed poly (vinylidene fluoride) microparticles for tissue engineering applications," *Rsc Advances*, vol. 4, no. 62, pp. 33013–33021, 2014.
[34] L. M. M. Costa, R. E. S. Bretas, and R. Gregorio, "Effect of solution concentration on the electrospray/electrospinning transition and on the crystalline phase of PVDF," *Materials Sciences and Applications*, vol. 1, no. 04, p. 247, 2010.
[35] A. S. Macedo *et al.*, "Tailoring electroactive poly (vinylidene fluoride-co-trifluoroethylene) microspheres by a nanoprecipitation method," *Materials Letters*, vol. 261, p. 127018, 2020.
[36] M. Dong, M. Hafezi, Z. Tong, and L. Qin, "Preparation and oil lubrication of polyvinylidene fluoride (PVDF) nanospheres," *Materials Research Express*, vol. 6, no. 8, p. 85093, 2019.
[37] G. M. Whitesides, "The origins and the future of microfluidics," *Nature*, vol. 442, no. 7101, p. 368, 2006.
[38] S.-Y. Teh, R. Lin, L.-H. Hung, and A. P. Lee, "Droplet microfluidics," *Lab on a Chip*, vol. 8, no. 2, pp. 198–220, 2008.

[39] S. Xu *et al.*, "Generation of monodisperse particles by using microfluidics: control over size, shape, and composition," *Angewandte Chemie International Edition*, vol. 44, no. 5, pp. 724–728, 2005.
[40] C. A. Serra and Z. Chang, "Microfluidic-assisted synthesis of polymer particles," *Chemical Engineering & Technology: Industrial Chemistry-Plant Equipment-Process Engineering-Biotechnology*, vol. 31, no. 8, pp. 1099–1115, 2008.
[41] M. Brzeziński, M. Socka, and B. Kost, "Microfluidics for producing polylactide nanoparticles and microparticles and their drug delivery application," *Polymer International*, vol. 68, no. 6, pp. 997–1014, 2019.
[42] C.-H. Choi, J.-H. Jung, Y. W. Rhee, D.-P. Kim, S.-E. Shim, and C.-S. Lee, "Generation of monodisperse alginate microbeads and in situ encapsulation of cell in microfluidic device," *Biomed Microdevices*, vol. 9, no. 6, pp. 855–862, 2007.
[43] F. Heshmatnezhad and A. R. S. Nazar, "On-chip controlled synthesis of polycaprolactone nanoparticles using continuous-flow microfluidic devices," *Journal of Flow Chemistry*, vol. 10, no. 3, pp. 533–543, 2020.
[44] L. Xiong, P. Chen, and Q. Zhou, "Adhesion promotion between PDMS and glass by oxygen plasma pre-treatment," *Journal of Adhesion Science and Technology*, vol. 28, no. 11, pp. 1046–1054, 2014.
[45] P. Martins, C. M. Costa, M. Benelmekki, G. Botelho, and S. Lanceros-Mendez, "On the origin of the electroactive poly (vinylidene fluoride) β-phase nucleation by ferrite nanoparticles via surface electrostatic interactions," *CrystEngComm*, vol. 14, no. 8, pp. 2807–2811, 2012.
[46] J. J. Vaca-González *et al.*, "Effect of electrical stimulation on chondrogenic differentiation of mesenchymal stem cells cultured in hyaluronic acid–Gelatin injectable hydrogels," *Bioelectrochemistry*, vol. 134, p. 107536, 2020.
[47] R. Seemann, M. Brinkmann, T. Pfohl, and S. Herminghaus, "Droplet based microfluidics," *Reports on progress in physics*, vol. 75, no. 1, p. 16601, 2011.
[48] Y. Gao, C.-X. Zhao, and F. Sainsbury, "Droplet shape control using microfluidics and designer biosurfactants," *Journal of Colloid and Interface Science*, vol. 584, pp. 528–538, 2021.
[49] V. F. Cardoso, G. Botelho, and S. Lanceros-Méndez, "Nonsolvent induced phase separation preparation of poly (vinylidene fluoride-co-chlorotrifluoroethylene) membranes with tailored morphology, piezoelectric phase content and mechanical properties," *Materials & Design*, vol. 88, pp. 390–397, 2015.
[50] C. Ribeiro *et al.*, "Electroactive poly (vinylidene fluoride)-based structures for advanced applications," *Nat Protoc*, vol. 13, no. 4, p. 681, 2018.
[51] X. Cai, T. Lei, D. Sun, and L. Lin, "A critical analysis of the α, β and γ phases in poly (vinylidene fluoride) using FTIR," *RSC Adv*, vol. 7, no. 25, pp. 15382–15389, 2017.
[52] P. Martins, A. C. Lopes, and S. Lanceros-Mendez, "Electroactive phases of poly (vinylidene fluoride): Determination, processing and applications," *Prog Polym Sci*, vol. 39, no. 4, pp. 683–706, 2014.
[53] L. Ruan, X. Yao, Y. Chang, L. Zhou, G. Qin, and X. Zhang, "Properties and Applications of the β Phase Poly (vinylidene fluoride)," *Polymers (Basel)*, vol. 10, no. 3, p. 228, 2018.

[54] E. Lizundia, A. Reizabal, C. M. Costa, A. Maceiras, and S. Lanceros-Méndez, "Electroactive γ-Phase, Enhanced Thermal and Mechanical Properties and High Ionic Conductivity Response of Poly (Vinylidene Fluoride)/Cellulose Nanocrystal Hybrid Nanocomposites," *Materials*, vol. 13, no. 3, p. 743, 2020.
[55] S. Barrau *et al.*, "Nanoscale investigations of α-and γ-crystal phases in PVDF-based nanocomposites," *ACS Appl Mater Interfaces*, vol. 10, no. 15, pp. 13092–13099, 2018.
[56] W. M. Prest Jr and D. J. Luca, "The formation of the γ phase from the α and β polymorphs of polyvinylidene fluoride," *Journal of Applied Physics*, vol. 49, no. 10, pp. 5042–5047, 1978.
[57] R. Hasegawa, M. Kobayashi, and H. Tadokoro, "Molecular conformation and packing of poly (vinylidene fluoride). Stability of three crystalline forms and the effect of high pressure," *Polymer Journal*, vol. 3, no. 5, pp. 591–599, 1972.
[58] T. Nishiyama, T. Sumihara, Y. Sasaki, E. Sato, M. Yamato, and H. Horibe, "Crystalline structure control of poly (vinylidene fluoride) films with the antisolvent addition method," *Polymer Journal*, vol. 48, no. 10, pp. 1035–1038, 2016.
[59] K. M. Kim, W. S. Jeon, N.-G. Park, K. S. Ryu, and S. H. Chang, "Effect of evaporation temperature on the crystalline properties of solution-cast films of poly (vinylidene fluoride) s," *Korean Journal of Chemical Engineering*, vol. 20, no. 5, pp. 934–941, 2003.
[60] P. Martins, A. Lasheras, J. Gutiérrez, J. M. Barandiaran, I. Orue, and S. Lanceros-Mendez, "Optimizing piezoelectric and magnetoelectric responses on CoFe2O4/P (VDF-TrFE) nanocomposites," *Journal of Physics D: Applied Physics*, vol. 44, no. 49, p. 495303, 2011.
[61] A. C. Lopes, C. M. Costa, C. J. Tavares, I. C. Neves, and S. Lanceros-Mendez, "Nucleation of the electroactive γ phase and enhancement of the optical transparency in low filler content poly (vinylidene)/clay nanocomposites," *The Journal of Physical Chemistry C*, vol. 115, no. 37, pp. 18076–18082, 2011.
[62] V. N. Bliznyuk, A. Baig, S. Singamaneni, A. A. Pud, K. Y. Fatyeyeva, and G. S. Shapoval, "Effects of surface and volume modification of poly (vinylidene fluoride) by polyaniline on the structure and electrical properties of their composites," *Polymer (Guildf)*, vol. 46, no. 25, pp. 11728–11736, 2005.
[63] Z. Wojnarowska *et al.*, "Molecular dynamics, physical stability and solubility advantage from amorphous indapamide drug," *Mol Pharm*, vol. 10, no. 10, pp. 3612–3627, 2013.
[64] D. M. Correia *et al.*, "Crystallization Monitoring of Semicrystalline Poly (vinylidene fluoride)/1-Ethyl-3-methylimidazolium Hexafluorophosphate [Emim][PF6] Ionic Liquid Blends," *Crystal Growth & Design*, vol. 21, no. 8, pp. 4406–4416, 2021.
[65] D. M. Correia *et al.*, "Influence of cation and anion type on the formation of the electroactive β-phase and thermal and dynamic mechanical properties of poly (vinylidene fluoride)/ionic liquids blends," *The Journal of Physical Chemistry C*, vol. 123, no. 45, pp. 27917–27926, 2019.
[66] M. Salmerón Sánchez, V. B. F. Mathot, G. vanden Poel, and J. L. Gómez Ribelles, "Effect of the cooling rate on the nucleation kinetics of poly (L-lactic acid) and its influence on morphology," *Macromolecules*, vol. 40, no. 22, pp. 7989–7997, 2007.

[67] R. Gregorio Jr, "Determination of the α, β, and γ crystalline phases of poly (vinylidene fluoride) films prepared at different conditions," *Journal of Applied Polymer Science*, vol. 100, no. 4, pp. 3272–3279, 2006.
[68] L. Ourry, S. Marchesini, M. Bibani, S. Mercone, S. Ammar, and F. Mammeri, "Influence of nanoparticle size and concentration on the electroactive phase content of PVDF in PVDF–CoFe2O4-based hybrid films," *physica status solidi (a)*, vol. 212, no. 2, pp. 252–258, 2015.
[69] G. Botelho, S. Lanceros-Méndez, A. M. Gonçalves, V. Sencadas, and J. G. Rocha, "Relationship between processing conditions, defects and thermal degradation of poly (vinylidene fluoride) in the β-phase," *J Non Cryst Solids*, vol. 354, no. 1, pp. 72–78, 2008.
[70] R. Gonçalves *et al.*, "Nucleation of the electroactive β-phase, dielectric and magnetic response of poly (vinylidene fluoride) composites with Fe2O3 nanoparticles," *J Non Cryst Solids*, vol. 361, pp. 93–99, 2013.
[71] K. Mitsuda, H. Kimura, and T. Murahashi, "Evaporation and decomposition of Triton X-100 under various gases and temperatures," *J Mater Sci*, vol. 24, no. 2, pp. 413–419, 1989.
[72] K.-H. Cho, M. I. Bichurin, V. M. Petrov, A. Bhalla, and S. Priya, "Magnetoelectric Laminate Composite: Effect of Piezoelectric Layer on Magnetoelectric Properties," *Ferroelectrics*, vol. 473, no. 1, pp. 110–128, 2014.
[73] A. Wickens and J. Robinson, "Magnetoelectric Neural Modulation," *Biophysical Journal*, vol. 112, no. 3, p. 286a, 2017.

Table of Contents

EQUATION 1 12

EQUATION 2 13

EQUATION 3 15

EQUATION 4 16

EQUATION 5 17

FIGURE 1 – A) MICROFLUIDIC FLOW-FOCUSING DEVICE, B) DEVICE'S CHANNEL DIMENSION C) PVDF AND PVDF-CFO MICROSPHERE PRODUCTION SCHEME 4

FIGURE 2 – FESEM IMAGES OF A) VARIOUS PVDF MICROSPHERES, B, C) PVDF AND PVDF-CFO MICROSPHERES, RESPECTIVELY, WITH INSETS OF SURFACE DETAILS, AND D, E) A FIB CROSS-SECTIONED PVDF-CFO MICROSPHERE. 8

FIGURE 3 – HISTOGRAMS OF PVDF AND PVDF-CFO MICROSPHERE DIAMETER FOR THE DIVERSE PROCESSING PARAMETERS (N=50) (TOP), MICROSPHERE DIAMETER DEPENDENCE ON PROCESSING PARAMETERS (BOTTOM) 10

FIGURE 4 - FTIR SPECTRA FOR THE PVDF AND PVDF-CFO MICROSPHERES. ORIGINAL PVDF PELLETS SPECTRUM IS ALSO SHOWN FOR COMPARISON 11

FIGURE 5 - FTIR SPECTRA DECONVOLUTION FOR A) PVDF AND B) PVDF-CFO MICROSPHERES BETWEEN 1140-1300CM^{-1}. 12

FIGURE 6 - A) DSC SPECTRA FOR THE PVDF AND PVDF-CFO MICROSPHERES, B) TGA SPECTRA FOR THE PVDF AND PVDF-CFO MICROSPHERES 14

FIGURE 7 - HYSTERESIS LOOP FOR PVDF-CFO MICROSPHERES AND INSET FOR PURE CFO. 17

FIGURE 8 - MTS RELATIVE METABOLIC ACTIVITY FOR PVDF AND PVDF-CFO MICROSPHERES AT 24 AND 72 H CULTURE TIMES. 18

TABLE 1 - PVDF AND CORRESPONDING CRYSTAL PHASE IR SPECIFIC PEAKS. 12

TABLE 2 - THERMAL PARAMETERS AND CONTENT OF CRYSTAL PHASES OF PVDF AND PVDF-CFO.MICROSPHERES 15

Support material